Macromolecules

ARTICLE

pubs.acs.org/Macromolecules

Structuring of Polyelectrolyte (NaPSS) Solutions in Bulk and under Confinement as a Function of Concentration and Molecular Weight

Cagri Üzüm, Stephanie Christau, and Regine von Klitzing*

Stranski-Laboratorium, Institut für Chemie, Technische Universität Berlin, Strasse des 17. Juni 124, D-10623 Berlin, Germany

ABSTRACT: The present paper gives a deeper insight into the chain ordering in aqueous polyelectrolyte solutions under geometrical confinement as a function of degree of polymerization and polymer concentration. Colloidal probe atomic force microscopy (CP-AFM) and small-angle X-ray scattering (SAXS) are used to compare the poly(styrenesulfonate) (NaPSS) chain ordering between two solid interfaces and in bulk, respectively. Oscillatory force−distance curves from CP-AFM as well as the scattering peaks from SAXS indicate a near range ordering of polyelectrolyte chains with structural parameters such as interchain distance, correlation length, and the strength of ordering. These characteristic lengths from CP-AFM (confinement) and SAXS (bulk) are in the same range. The interchain distance is up to 20% smaller and the correlation length is up to 20% higher under confinement, indicating a slight compression of the polyelectrolyte chains and a stronger counterion condensation under confinement. The interchain distance d scales with the monomer unit concentration c as $d \sim c^{-1/3}$ for a degree of polymerization N from 20 to 155 and as $d \sim c^{-1/2}$ for N = 367 and 10 690, indicating a dilute and semidilute regime, respectively. The transition from dilute to semidilute regime is in good agreement with the one found in viscosity measurements and with theoretical concepts. At a fixed monomer concentration, d depends on the chain length in the dilute regime while it is independent of the molecular weight in the semidilute regime. The experimental intercoil distance d in the dilute regime coincides well with the one calculated from the coil number density, which is based in turn on a theoretical model. Other models for calculating the interchain distance are discussed. The correlation length of the ordering increases with increasing molecular weight, indicating an increase in counterion condensation. The strength of ordering increases with the degree of polymerization due to entropic reasons.

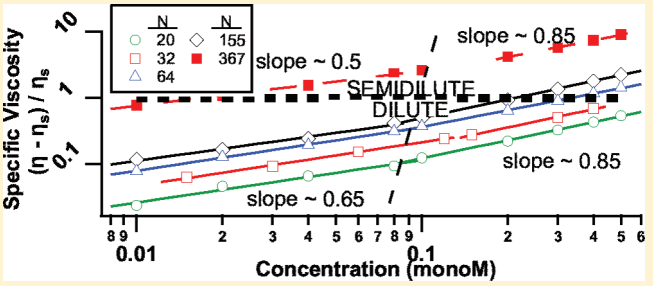

1. INTRODUCTION

In addition to their high solubility and nontoxic nature, polyelectrolytes can be destabilized simply by adding salt in the system. Therefore, they are widely used as flocculants and stabilizers in colloidal suspensions as well as in emulsions and foams. With respect to e.g. colloidal (de)stabilization or microfluidics, the structuring of polyelectrolytes is important. In aqueous systems, structuring of polyelectrolyte solutions is known to be highly concentration dependent.[1−6] Below a critical overlap concentration c^* polyelectrolyte chains do not overlap, and they form individual coils, still interacting with each other. This concentration range ($c < c^*$) is referred to as the dilute regime, and the isotropic model suggests that the interchain distance (or the intercoil distance in this case) scales with the concentration as $c^{-1/3}$. This scaling is typical for 3D particle packing[7−11] as a rough representation can be seen in Figure 1a. For $c > c^*$, however, a structural change is predicted by theory.[1−4,6,12−16] At c^*, polyelectrolyte chains start to overlap and form a transient mesh-like structure that is not fully entangled (see Figure 1b). Mesh-like structures, i.e., transient networks, keep their existence in a specific concentration range, the so-called unentangled−semidilute regime. In this regime, the interchain distance (or the mesh size) scales with the concentration as $c^{-1/2}$. According to Milling and Kendall,[17] Theodoly et al.,[18] and Jönsson et al.,[19] however, polyelectrolyte chains form parallel aligned lateral layers rather than mesh-like networks. A recent molecular level study indicated that a transition between a lateral layer structure and a network structure is possible.[20] Finally, when the polyelectrolyte concentration reaches a second critical concentration called the entanglement concentration, $c^{**} \approx 1000c^*$, the chains lose their fairly defined ordering and start to randomly entangle. This concentration regime is referred to as entangled−semidilute regime and has different rheological properties than the dilute or unentangled−semidilute regime.[4,6,21,22]

A number of experimental techniques such as small-angle scattering (SAXS and SANS)[18,23−31] and dynamic light scattering (DLS)[32−35] have been used to study the polyelectrolyte solutions in bulk. A distinguishing bulk property of polyelectrolytes, which the neutral polymers lack of, is that SAXS or SANS measurements on polyelectrolyte solutions present broad structure peaks. The peak position, q_{max}, can be used to determine the interchain distance in bulk using the Bragg equation $d = 2\pi/q_{max}$.

Polyelectrolyte systems possess not only unique bulk properties but also interesting interchain interactions in thin-film geometry. Understanding these interactions is the key to understanding the

Received: June 28, 2011
Revised: August 29, 2011
Published: September 16, 2011

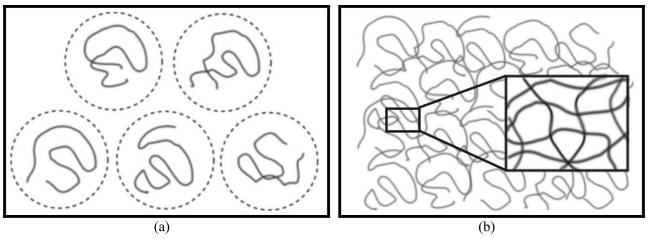

Figure 1. A rough representation of chain conformation in (a) dilute and (b) unentangled−semidilute regimes.

macroscopic properties (e.g., rheology and stability) of the system. Studying thin films of aqueous polyelectrolyte solutions experimentally is also necessary to complement the intense theoretical effort focusing on the microscopic behavior of the system such as ion distribution and chain conformation. Confined polyelectrolyte systems can be studied with several techniques including surface force apparatus (SFA),[36] total internal reflection microscopy (TIRM),[36,37] optical tweezers,[36] thin film pressure balance (TFPB),[18,29,38−43] and colloidal-probe atomic force microscopy (CP-AFM).[17,30,31,43−49] There is a number of recent reviews focusing on the experimental determination of the structural forces in polyelectrolyte or similar systems.[36,50−53] The film disjoining pressure profile in TFPB and the force curves in AFM show oscillatory behavior as the confining opposing interfaces are approached down to a distance of several times the interchain distance. This is explained by a layerwise expulsion of polyelectrolyte chains from the confinement, and the period of the oscillations gives therefore the interchain distance in the confined geometry.[54] In contrast to e.g. TFPB, CP-AFM allows accurate measurement of both the repulsive and attractive interactions between two surfaces. Therefore, it was used in this study to monitor the oscillatory structural forces in polyelectrolyte solutions.

It was reported that there is no or negligible difference between the characteristic lengths of bulk and thin-film structuring of linear polyelectrolytes.[18,29−31,41] In contrast to this, simulations show that in a physical confinement the structuring of the polymer chains is affected by the chain length and can be different from the bulk, so that the number ratio of shorter and longer chains changes depending on the degree of confinement due to their different translational entropies.[55,56] Comparisons of solutions containing monodisperse polyelectrolytes, each with different chain lengths, were previously performed in bulk for poly(acrylic acid)[17] and NaPSS,[25,28,32,34] in thin-film geometry for poly(acrylic acid),[17,57] NaPSS,[44,58] and supramolecular polymers,[47,48] and in both geometries for PDADMAC.[29] All are reporting more or less chain length dependent structural properties. Recently, Biggs et al. experimentally showed for binary solutions of short and long NaPSS chains that the shorter chains dominate the structuring under confinement restricted that they are in the dilute regime while the longer chains are in the semidilute one.[59]

Literature still lacks of studies on the effect of confinement on the transition from dilute to semidilute regime, which will be one of the main focuses of the current work. The intention was to check if it is possible to trigger a structural change in the polyelectrolyte system by entrapping it in a thin-film geometry. Solutions of highly monodisperse NaPSS were chosen as a model system. The chain length in scope ranges from ∼20 monomers to ∼11 000 monomers per chain in a monomer concentration regime of 0.01−0.5 mol/L (M). For a comparison between the structural behavior in bulk and confined geometry, SAXS and CP-AFM techniques were used, respectively. The experimental results were compared to the calculated ones from particle number density and from scaling theory.[4] Rheological properties of the samples were investigated to correlate the microscopic structuring of the polymers to their macroscopic behavior.

2. EXPERIMENTAL SECTION

2.1. Materials. The poly(styrenesulfonic acid sodium salt) (NaPSS) samples with the molecular weights 4219, 6530, 13 200, 32 000, 75 600, and 2 260 000 g/chain corresponding to chain lengths of N = 20, 32, 64, 155, 366, and 10 960, respectively, were purchased from Sigma-Aldrich (Product Nos. 81606, 81607, 81608, 81610, 81612, and 81617 and the polydispersity index M_w/M_n = 1.05, 1.06, 1.04, 1.04, 1.02, and 1.02, respectively). The solutions were prepared in Milli-Q (Millipore) water without any further purification. The concentration values refer to the respective monomer concentrations.

2.2. Methods. *2.2.1. Colloidal Probe Atomic Force Microscopy (CP-AFM).* The colloidal probe technique developed by Ducker et al.[60] was used throughout the study to study the effect of the confinement. A spherical silica particle is glued with epoxy to a tipless cantilever with a given spring constant of 0.03−0.08 N/m (CSC12, Micromasch). Silica particles with a radius R of about 3.35 μm were purchased from Bangs Laboratories, Inc. The cantilevers carrying the colloidal probes were exposed to air plasma cleaning for 20 min to remove all the organic components on their surface. The substrate used is a silicon wafer with a native SiO_2 top layer, cleaned with the RCA method,[61] and stored in Milli-Q water. Just before each experiment, the substrate was taken out of the water and dried in a nitrogen stream. Then a drop of the target polymer solution was put onto the substrate, and the probing head was fully immersed in the solution. Force−separation curves were collected via a commercial atomic force microscope MFP3D (Asylum Research, Inc.). Forces between the microsphere and the planar substrate are considered as forces between two planar surfaces (Derjaguin approximation) since the distance between the probe and the substrate is much smaller than the radius of the probe. No adsorption of the NaPSS is expected as both the polymer chains and the SiO_2 surfaces are negatively charged in the experimental conditions. 15 to 25 force−distance curves were taken at different positions on the same substrate as well as on different substrates with different cantilevers for better statistics. For the analysis, the oscillatory force−separation curves obtained by colloidal probe AFM were fitted with the formula[30,31,46]

$$\frac{F(x)}{2\pi R} = A^{-\lambda x}\cos[2\pi(x/d) + \varphi] + \mathit{offset} \quad (1)$$

Here, $F(x)$ is the force as a function of the separation between the two confining walls x, R is the radius of the colloidal probe, A is the amplitude, and λ is the decay length of the oscillation. d corresponds to the period of the oscillation while φ (phase shift) and *offset* are the correction parameters. φ and *offset* will not be discussed any further. It should be noted that while fitting the force data, the region very close to hard contact (x < 10 nm) should not be included due to additional contribution of the nonstructural forces.

2.2.2. Small-Angle X-ray Scattering (SAXS). SAXS measurements were performed using a SAXSess mc^2 system (Anton Paar KG, Austria) equipped with a sealed tube microsource and a line collimator, operated at 40 kV and 50 mA, producing Cu Kα radiation having a wavelength of 0.154 nm. Data treatment was done using SAXSquant 3.5 (Anton Paar, Austria) and Igor Pro (Wavemetrics) software packages. The background subtracted data were desmeared against the beam length profile of the source. Samples were measured in a 1 mm quartz capillary at 25 °C. The peak position q_{max}, the full width at half-maximum Δq, and

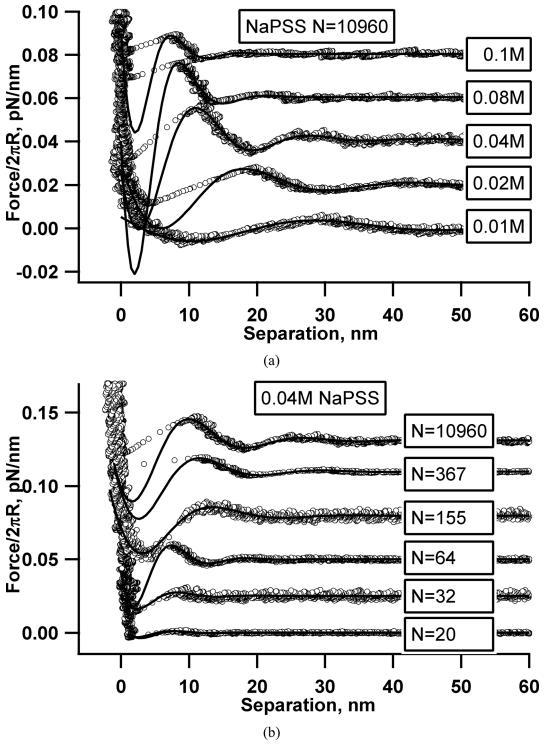

Figure 2. Force−separation curves obtained by CP-AFM (a) for $PSS_{N=10960}$ at different monomer concentrations and (b) for various N at a fixed monomer concentration of 0.04 M. Solid lines represent the extrapolated fits according to eq 1.

the maximum intensity of the scattering curves I_{max} were determined by a Lorentzian fitting of the scattering pattern around the peak area, as was previously suggested.[30,31,62] An approximate average error of ±15% for all these three parameters was calculated from the standard deviation of the fits as reflects to the relevant graphs.

2.2.3. Viscosity Measurements. The viscosity of the polyelectrolyte solutions was measured by the commercial Processor Viscosity System PVS1 (Lauda, Germany) using a Micro-Ubbelohde glass capillary viscometer (Schott, Germany) with a viscometer constant of 0.010 05 mm^2 s^2. The flow time was detected by two infrared sensors, and the analysis was made by the relevant Lauda software.

3. RESULTS AND DISCUSSION

Because of restrictions with respect to concentration regimes, CP-AFM and SAXS complement each other perfectly in a certain concentration range: in CP-AFM measurements, viscosity was observed to be crucial for the amplitude of the oscillatory curves, suppressing the oscillation peaks and giving a significant increase in noise, especially for $c > 0.1$ M. With SAXS also more concentrated systems can be studied. On the other hand, for lower concentrations ($c < 0.04$ M) it was not possible to get strong peaks with SAXS system that was used throughout the study.

The force between the two confining walls (silica sphere and the silicon substrate) was recorded using a CP-AFM as the separation between them is decreased continuously. The force−separation curves for various NaPSS solutions are presented in Figure 2. Solid lines show the fits of the recorded force curves according to eq 1, extrapolated for the separations smaller than 10−15 nm, where the interactions cannot be explained by this equation due to nonstructural forces. Equation 1 represents the

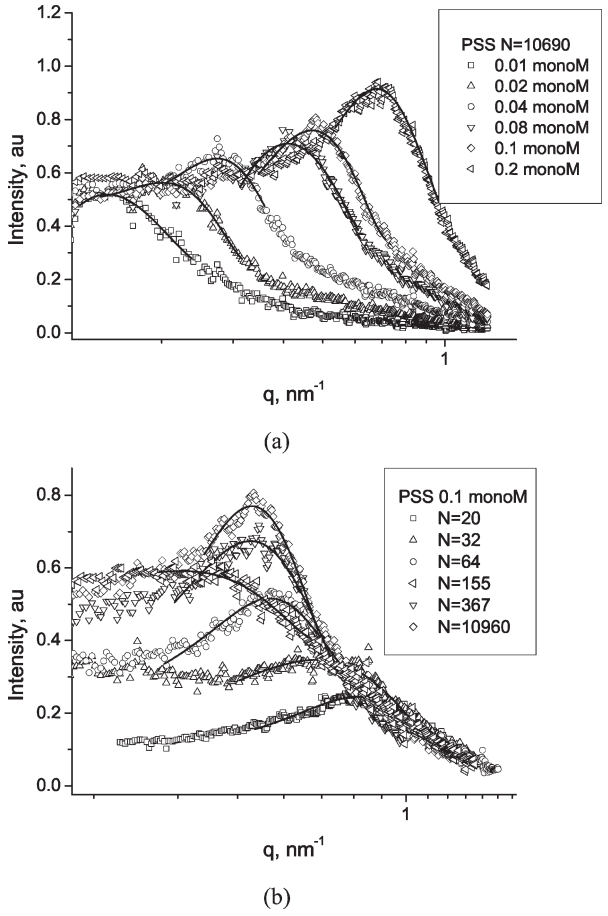

Figure 3. Scattering patterns obtained by SAXS (a) for $PSS_{N=10690}$ at different monomer concentrations and (b) for various N at a fixed monomer concentration of 0.1 M. Solid lines represent the Lorentzian fits as was previously suggested.[31]

asymptotic pair correlation function in bulk, i.e., for infinite distance.[8,63] It was however shown to be valid in nanoparticle systems under confinement as well.[7,8] For NaPSS with the molecular weight 2 260 000 g/chain (N = 10 960), Figure 2a shows that the oscillations become more pronounced and the period of the oscillation decreases with increasing monomer concentration. This behavior was observed for all other studied chain lengths as well. Figure 2b shows the force curves for different degrees of polymerization N at a fixed monomer concentration of 0.04 M (an average concentration at which the force−separation data can be reasonably fitted). Not only at this concentration but also in the whole studied concentration range, longer chains present more pronounced peaks. From the fitting curves, d, λ, and A were extracted, which correspond to the interchain distance, the correlation length, and the interaction strength in the system, respectively.

The SAXS spectra for the respective polyelectrolyte solutions are shown in Figure 3. The SAXS data show a maximum in the scattering intensity, indicating at least a near range ordering. Figure 3a shows the SAXS spectra for NaPSS with a fixed chain length of N = 10 960. With increasing monomer concentration, the maximum scattering intensity I_{max} increases and the position of the peak maximum shifts to higher q values. This trend is the same also for other studied chain lengths. SAXS spectra at 0.1 M (an average concentration at which the scattering curves can be

reasonably fitted) NaPSS with different degrees of polymerization are presented in Figure 3b. The general trend is that the peak becomes more pronounced and the peak position shifts to lower q values with increasing chain length up to $N = 367$. For $N = 367$ and $N = 10\,690$, the peak position q_{max} is nearly the same while I_{max} is larger for $N = 10\,960$. This observation is valid also for other studied monomer concentrations. From the SAXS data, q_{max}, Δq, and I_{max} were extracted as was explained in the Experimental Section, with an average error of ±15%. $2\pi/q_{max}$ (interchain distance) and $2/\Delta q$ (correlation length) were compared to d and λ from the CP-AFM data, respectively.

3.1. Interchain Distance: CP-AFM Period *d* vs SAXS $2\pi/q_{max}$. In a polyelectrolyte system, the period of the CP-AFM force−distance curves d and the reciprocal peak position in SAXS $2\pi/q_{max}$ correspond to the interchain distance in the thin-film geometry and in bulk, respectively. The dependence of thin film interchain distance d on the monomer concentration is shown in Figure 4a, as obtained from CP-AFM. For all chain lengths N, d decreases with increasing concentration and can be fitted with $d \sim c^{\alpha_{AFM}}$, α_{AFM} being the scaling exponent. Table 1 shows a summary of the α_{AFM} values for various N. For NaPSS samples with $N \approx 20$, 32, 64, and 155 (MWs 4219, 6530, 13 200, and 32 000, respectively), α_{AFM} is between −0.30 and −0.33. The exponent does not change systematically with N, and the average is close to $\alpha = -1/3$, which is the typical exponent for the ordering of objects in 3D. For relatively long chains with $N = 367$ and 10 960 (MWs 75 600 and 2 260 000) the interchain distance scales as $d \sim c^{-0.44}$ ($\alpha_{AFM} = -0.44$).

Figure 4b shows the bulk interchain distance $2\pi/q_{max}$ from SAXS against the monomer concentration for various N. In analogy to CP-AFM, $2\pi/q_{max}$ decreases with increasing concentration for all N with a dependence of $2\pi/q_{max} \sim c^{\alpha_{SAXS}}$, where α_{SAXS} is the scaling exponent. For $N = 20-155$, α_{SAXS} ranges between −0.29 and −0.38 giving an average close to $\alpha = -1/3$. For $N = 367$ and 10960 $\alpha_{SAXS} \approx -0.48$ and −0.49, which is close to the predicted value of −0.5 for network-like structure (see Table 1 for more detailed results). Figure 4c shows a comparison of the thin film and bulk interchain distances, d and $2\pi/q_{max}$, for all studied concentrations and chain lengths. It was observed that the difference between d and $2\pi/q_{max}$ is smaller than 20%, where $2\pi/q$ is always larger. The solid line in the plot shows the $d = 2\pi/q_{max}$ reference, and the dashed line is the fit of the whole data, giving that $d \approx 0.8 \times 2\pi/q_{max}$. Such a difference was not observed for other polyelectrolyte systems such as PAMPS.[31]

Before interpreting the scaling parameters α_{AFM} and α_{SAXS} in terms of chain structuring, the dependence of the interchain distance d or $2\pi/q_{max}$ on N should be emphasized. Figure 4a,b shows that the interchain distance increases with increasing N at a fixed monomer concentration, up to $N = 155$. For $N = 367$ and 10 960, however, the interchain distance is more or less the same at the same monomer concentration.

$\alpha \approx -1/3$ for particle-like systems and $\alpha \approx -1/2$ for polyelectrolyte mesh-like structures are suggested in a significant number of theoretical and experimental works as has been discussed in the Introduction. Therefore, $\alpha \simeq -0.44$ or $\simeq -0.5$ for $N = 367$ and 10 960 suggests a mesh-like structuring as was suggested by the theory[1,4] and was observed experimentally for different types of polyelectrolytes.[30,31,45,46] The independence of the interchain distance from N for $N = 367$ and 10 690 supports also a mesh-like structuring because in the semidilute regime, the chains are much longer than the mesh size of the network and their length does not affect the mesh size.[59]

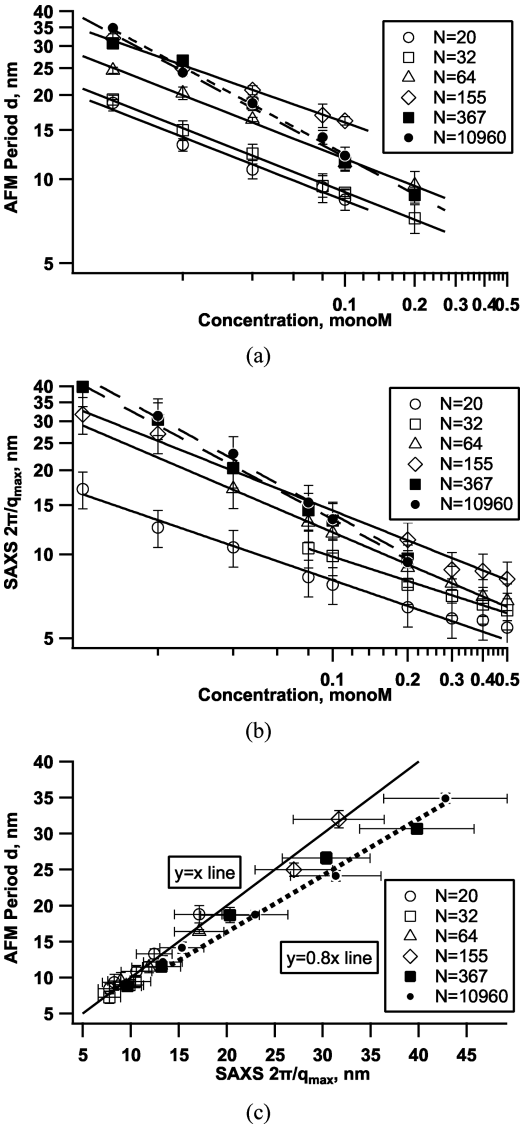

Figure 4. Concentration dependence of the interchain distance from (a) CP-AFM (d) and (b) SAXS ($2\pi/q_{max}$). The symbols are the measured values while the lines show the fits with the slope α. See Table 1 for the α values in the relations $d \sim c^{\alpha}$ and $2\pi/q_{max} \sim c^{\alpha}$. (c) Comparison of CP-AFM d vs SAXS $2\pi/q_{max}$. The symbols are the measured values, the dashed line is the linear fit of the whole data, and the solid line is the reference $d = 2\pi/q_{max}$ line.

For $N = 20$, 32, 64, and 155, $\alpha \sim -0.33$. The same scaling law as it has also been reported for silica nanoparticles,[7−11] potassium polyacrylate (KPAA),[64] and NaPSS[25] in dilute regime and for partially charged PSS[30] in semidilute regime. For fully charged NaPSS chains with a molecular weight of ≈35 000 g/chain, Biggs and co-workers reported a change in scaling from −0.5 to −0.33 for the last two depletion layers in the semidilute regime using the TIRM technique.[45] In the current study, this behavior could not be reproduced, since CP-AFM generally detects only the last two depletion layers. On the other hand, for the partially charged NaPSS, Qu et al.[30] suggested a percolation of the partially charged chains due to partial hydrophobicity, leading to a microdomain formation, i.e., pearl-necklace conformation.[30,65] In the present study, however, the reason for the particle-like behavior ($d \sim c^{-1/3}$) cannot be explained by partial hydrophobicity

dx.doi.org/10.1021/ma201466a |Macromolecules 2011, 44, 7782–7791

Table 1. α and β Values in the Relations $d \sim c^{\alpha_{AFM}}$, $2\pi/q_{max} \sim c^{\alpha_{SAXS}}$, $\lambda \sim c^{\beta_{AFM}}$, and $2/\Delta q \sim c^{\beta_{SAXS}}$ Depending on the Chain Length N

MW (g/mol)	N	α_{AFM}	α_{SAXS}	β_{AFM}	β_{SAXS}	regime
4219	20	-0.33 ± 0.03	-0.31 ± 0.02	-0.26 ± 0.07		dilute
6530	32	-0.33 ± 0.01	-0.29 ± 0.01	-0.28 ± 0.05		dilute
13200	64	-0.33 ± 0.01	-0.38 ± 0.01	-0.37 ± 0.03	-0.37 ± 0.03	dilute
32000	155	-0.30 ± 0.02	-0.35 ± 0.02	-0.43 ± 0.02	-0.40 ± 0.01	dilute
75600	367	-0.44 ± 0.03	-0.48 ± 0.02	-0.46 ± 0.03	-0.33 ± 0.02	semidilute
2260000	10960	-0.44 ± 0.03	-0.49 ± 0.02		-0.35 ± 0.04	semidilute

because for all studied samples under the scope, chains consist of the same sodium styrenesulfonate monomers (assuming a high degree of sulfonation and purity of the samples). The only reason for this particle-like behavior of the chains is that the solutions are still in the dilute regime, forming layers of coils. The existence of individual coils in the solution also explains the chain length dependence of the interchain distance for $N = 20-155$ at a fixed monomer concentration. The concentration of coils decreases with increasing chain length at a fixed monomer concentration, leading to an increase in coil−coil distance. The relation between the intercoil distance and radius of gyration of a single coil R_g will be discussed more in detail in the theoretical calculations section.

The results above indicate that, even with keeping the monomer concentration range constant, there can be a transition from dilute to unentangled−semidilute regime, depending on the polyelectrolyte chain length. Kaji et al.[25] and Nishida et al.[28] also reported a chain length dependent dilute−semidilute behavior, but Milling,[44] Biggs et al.,[58] and v. Klitzing et al.[29] observed no such transition. This lack of dilute−semidilute transition in the latter works can be explained by the narrower chain length or concentration range studied, because in order to see such a transition, the concentration range should be chosen such in a way that the overlap concentration would be reached only by the longer chains.

To summarize, for $N = 20-155$ $\alpha_{AFM} \simeq \alpha_{SAXS} \simeq -0.33$. For $N = 367$ and 10 690 $\alpha_{AFM} \simeq -0.44$ is a bit different than $\alpha_{SAXS} \simeq -0.5$. Confinement leads to structural oscillatory forces and a slight decrease of interchain distance, but it does not trigger a structural transition from dilute to semidilute (or vice versa) ordering, independent of the chain length.

3.2. Correlation Length: CP-AFM Decay Length λ vs SAXS Peak Width $2/\Delta q$. The decay length of the oscillatory force λ and the inverse width of the SAXS peak $2/\Delta q$ correspond to the correlation length for a polyelectrolyte system[30,31,62] in thin film geometry and in bulk, respectively. Analyzing these two parameters, one gathers information about the counterion distribution around the chains and the range of chain ordering. Figure 5a shows that λ decreases with increasing monomer concentration for all degrees of polymerization N. This behavior is a result of increasing counterion concentration with increasing c and was previously observed.[30,31] Figure 5a also shows that at a fixed monomer concentration λ increases with increasing N, suggesting that the chain length affects the counterion distribution around the chains as well as their conformation (see the previous section).

The correlation length in bulk was determined from the SAXS data. The reciprocal peak widths $2/\Delta q$ were calculated and were plotted against the monomer concentration for all N, as shown in Figure 5b. For the two shortest chain lengths ($N = 20$ and 32) the low scattering intensity of the SAXS patterns did not allow a reliable analysis of the peak width. For the other samples, a

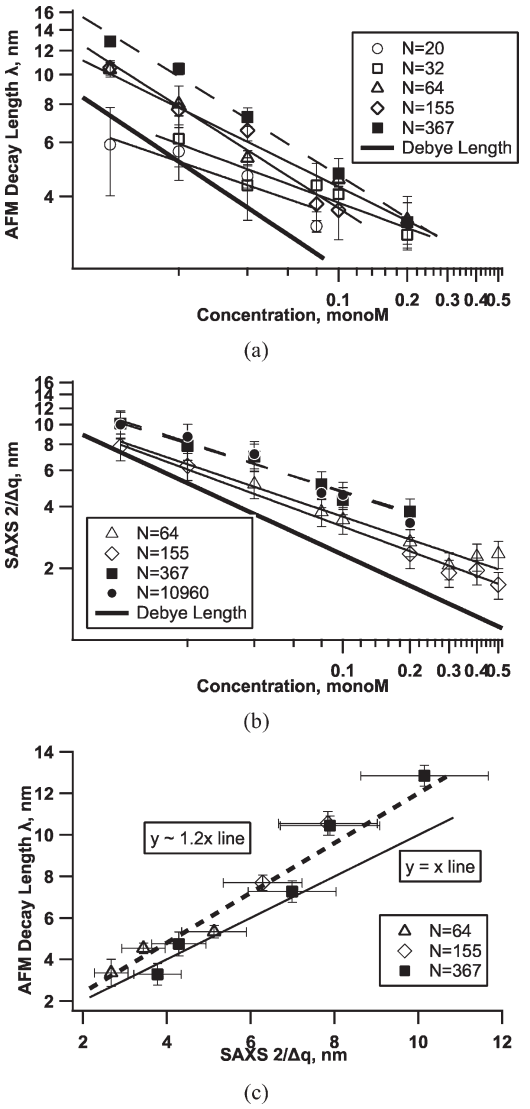

Figure 5. Concentration dependence of the (a) CP-AFM decay length λ and (b) SAXS $2/\Delta q$ in logarithmic scale. The lines show the fits with the slope β. See Table 1 for the β values in the relations $\lambda \sim c^{\beta}$ and $2/\Delta q \sim c^{\beta}$. (c) A comparison of the absolute correlation length values from the both techniques is shown. The solid line is the $\lambda = 2/\Delta q$ reference line, and the dashed line is the actual fit.

decreasing correlation length $2/\Delta q$ with increasing monomer concentration was observed as for CP-AFM measurements. The second observation from the CP-AFM that the correlation length decreases with decreasing N is also valid for SAXS, showing that this effect is not restricted to the thin film geometry.

dx.doi.org/10.1021/ma201466a |Macromolecules 2011, 44, 7782–7791

To get a deeper insight into the concentration and chain length effect on λ and $2/\Delta q$, the dependence of the decay length on the monomer concentration was expressed as $\lambda \sim c^{\beta_{AFM}}$ and $2/\Delta q \sim c^{\beta_{SAXS}}$, β being the scaling exponent. β can be determined from the slope of a linear fit on a log(correlation length)−log(c) plot. These fits are presented by solid or dashed lines in Figure 5a, b. Table 1 shows the β values calculated from the respective slopes.

In CP-AFM experiments, it was observed for the three dilute regime samples (N = 20, 32, 64) that β_{AFM} decreases from −0.26 to −0.37 with increasing N. NaPSS with N = 155 (in the dilute regime) and 367 (in the semidilute regime) have β_{AFM} = −0.43 and −0.46, respectively. The error bars in Figure 5a are not large enough to change the scaling law dramatically, but it should be noted that especially the solutions of the longest two chains (N = 367 and 10 960) are very viscous, resulting in noisy AFM force−distance curves and a more difficult fitting of the curves. Therefore, no reliable β_{AFM} value for N = 10 690 could be extracted. β_{SAXS} values were calculated in an analogical way, from the logarithmic slope of $2/\Delta q \sim c^{\beta_{SAXS}}$. β_{SAXS} can be seen as compared to β_{AFM} in Table 1. Except for N = 367, β_{AFM} and β_{SAXS} agree well, suggesting that the correlation lengths in thin film and in bulk are similar; in other words, confinement does not alter the ion distribution in NaPSS systems.

λ and $2/\Delta q$ have been correlated with the theoretical Debye length λ_D in the literature.[26,30,31] λ_D scales as $\sim c^{-1/2}$ and characterizes the counterion screening in solution.[31] It was reported both for NaPSS and PAMPS that λ and $2/\Delta q$ are closer to λ_D for lower charge fractions while for high charge fractions they can be up to twice the λ_D.[30,31] This was explained by the deviance by additional influences of the monomer−monomer interactions on the free energy of the system, for higher charge fractions. It was however reported that the experimental correlation length−concentration scaling remains as $\sim c^{-1/2}$ ($\beta_{AFM} \approx \beta_{SAXS} \approx -0.5$). In the current study, significant differences in absolute values of λ or $2/\Delta q$ and λ_D as well as their scaling with the concentration were observed. For the comparison, the experimental correlation lengths λ or $2/\Delta q$ and the calculated Debye lengths ($\lambda_D = 1/(4\pi l_b f_{eff} c)^{1/2}$, where the effective charge fraction f_{eff} = 35% due to Manning condensation[66] and the Bjerrum length l_b = 7.1 Å) are shown in Figure 5a,b. As was discussed above, the scaling parameters β_{AFM} and β_{SAXS} range between −0.26 and −0.37 rather than at −0.5 for N = 20, 32, and 64. The samples with N = 155 and 367 have β = −0.43 and −0.46, respectively, being the only samples more or less in agreement with the Debye length exponent of −0.5. It can be seen from Figure 5a,b that nearly for all chain lengths $\lambda \approx 2/\Delta q > \lambda_D$. This result agrees with the previous experimental reports discussed above[26,30,31] and the theory[4] that the screening length is proportional to but larger than the Debye length around c^*. How the Debye length λ_D and the correlation length (λ and $2/\Delta q$) is related to the interchain distance (d or $2\pi/q_{max}$) will be discussed below in the theoretical calculations section.

Figure 5c presents a comparison of absolute values of CP-AFM λ and SAXS $2/\Delta q$. The solid line is the reference $\lambda = 2/\Delta q$ line, and the dashed line is the actual fit of the whole data showing that $\lambda \approx 1.2 \times 2/\Delta q$. For shorter chains (smaller correlation lengths) as well as lower concentrations (larger correlation lengths), the deviation between two parameters increases, λ being mostly larger. As has been discussed for the interchain distances, very low concentrations in SAXS and very high concentrations in CP-AFM lowers the quality of analysis. This should be kept in mind while attributing these differences to any ion distribution difference between bulk and confined regions.[30,31,46]

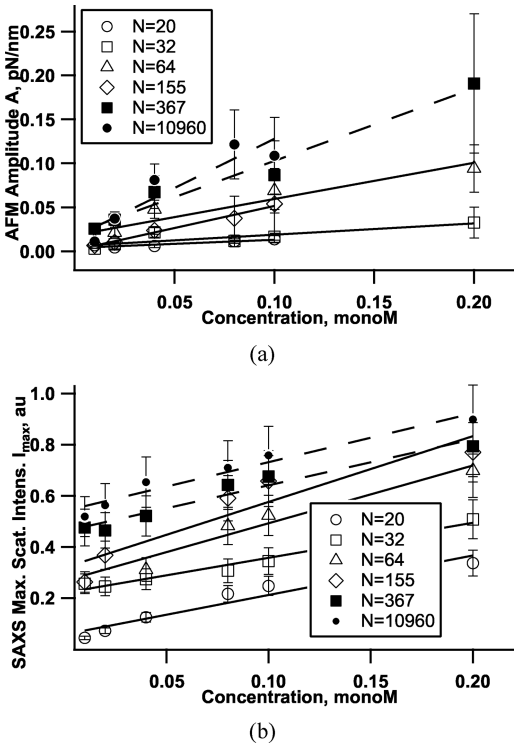

Figure 6. Concentration dependence of the (a) CP-AFM amplitude A and (b) SAXS maximum intensity I_{max}. The solid lines show the linear fits.

Finally, a significant chain length dependence of λ and $2/\Delta q$ can be observed in Figure 5 as was discussed above. Although there is the same amount of monomers (or charges) in all systems with the same monomer concentration, λ and $2/\Delta q$ systematically increase with increasing chain length. Under the assumption that λ and $2/\Delta q$ would increase with decreasing counterion concentration, that would be a hint that in case of longer chains the amount of free counterions is reduced; in other words, an increase in molecular weight leads to an increase in counterion condensation. Increasing correlation length with increasing N can also be explained entropically so that lower translational entropy of the longer chains result in a less disordered structure.

3.3. Interaction Strength: CP-AFM Amplitude *A* and SAXS Peak Intensity I_{max}. The amplitude A of the oscillatory force−separation curves and the maximum scattering intensity I_{max} in SAXS are a measure of the strength of interchain repulsion. A and I_{max} were determined as was described in the Experimental Section. Figure 6a,b shows A and I_{max} for various monomer concentrations and N. First, A and I_{max} increase with increasing monomer concentration for a fixed N. This behavior was observed in other studies for several polyelectrolytes[17,29−31,44−46,51,54,67] and colloidal systems,[11] and it is an outcome of increasing total chain charge in the system. Actually, the interactions of the neighboring chains is created by the competition of electrostatic repulsion between the charges on the chains and the counteracting screening of the counterions created during the dissociation in the solution. If the charge fraction is high enough, the electrostatic repulsion dominates the interactions between the chains, leading to stronger repulsions for higher concentrations.

dx.doi.org/10.1021/ma201466a |*Macromolecules* 2011, 44, 7782–7791

Table 2. Polyelectrolyte Overlap and Entanglement Concentrations (c^* and c^{**}, Respectively) as a Function of Chain Length, N, As Calculated by eq 2[a]

N	c^* (monoM)	c^{**} (monoM) ($\geq$)
20	5.8	5.8×10^{3}
32	2.3	2.3×10^{3}
64	5.7×10^{-1}	5.7×10^{2}
155	9.7×10^{-2}	9.7×10^{1}
367	1.7×10^{-2}	1.7×10^{1}
10 960	1.9×10^{-5}	1.9×10^{-2}

[a] For a wider range of N dependence of c^*, see the work of Dobrynin et al.[4]

Second, it can be seen that A and I_{max} increase with increasing N at a fixed monomer concentration. This result agrees with the previously discussed observation that the correlation length increases with increasing N, meaning that due to their lower counterion concentration and lower translational entropy, longer chains have less disordered structuring and interact stronger with each other.

3.4. Comparison with the Theoretical Calculations. As was discussed in section 3.1, for the same monomer concentration range, the shorter chains with N = 20, 32, 64, and 155 are in the dilute regime while the longer two with N = 367 and 10 960 are in the unentangled−semidilute regime. This result is expected considering the fact that the overlap concentration c^* of short chains can be several orders of magnitude higher than that of relatively longer ones. According to the theory,[1,4,6] in the low salt concentration limit $c^* \sim N^{-2}$, restricted that the number of monomers in an electrostatic blob is the same for all chain lengths. The theoretical overlap concentrations c^* for NaPSS with different chain lengths is calculated based on the equations given by Dobrynin et al.[4] It should be noted that the parameters calculated by these equations were observed to deviate slightly from the simulation results, especially for smaller N.[5,6] According to these equations, c^* is given as

$$c^* \approx K^3 b^{-3} N^{-2} \tag{2}$$

where

$$K \approx (J^2/u)^{2/3}\tau, \quad \text{for NaPSS in water} \tag{3}$$

Here b is the monomer size (2.5 Å), J is the average number of monomers between charges, u is the ratio of Bjerrum length to the monomer size ($\approx$3), and τ is the reduced temperature. $J \approx 5$ and $K \approx 2.8$ were found by Dobrynin et al. for NaPSS in water, after comparing the equations with some experimental data,[4] and these values were used for the following calculations.

A summary of N vs c^* calculated from eq 2 is given in Table 2 in addition to the semidilute−unentangled to semidilute−entangled crossover concentration c^{**}, which is expected to be around 1000 times higher than c^*.[4,22] According to these results, for the NaPSS samples with N = 20, 32, 64, 367, and 10 960, no transition from dilute to semidilute regime is expected in the studied concentration regime (0.01−0.5 M). For N = 155, however, the slope of the log(c) vs log(d) should change from −1/3 to −1/2 at around 0.1 M. No such transition could be observed, probably due to the uncertainties in the theoretical parameters, but the data in Table 2 agree totally with the experimental results that shorter chains (N = 20−155) have $\alpha \sim -1/3$ rather than −1/2 and are in the dilute regime.

As it was mentioned in section 3.1, the interchain distance depends on N for the samples in the dilute regime (N = 20−155) while it is independent of N in the semidilute regime. In the case of concentrated suspensions of hard spherical particles, the distance between two particles was reported to be larger than the particle diameter and comparable to twice the sum of particle radius and the electrostatic Debye length λ_D.[68,69] It is then reasonable to assume that the distance between two polyelectrolyte coils should also be in the order of twice the sum of R_g and the λ_D, once λ_D is considered as the distance from the outer surface of the polyelectrolyte coil to the point where the electric field is mostly screened out. This assumption should be approached carefully as there is counterions also *inside* the coil. R_g of a polyelectrolyte chain in the dilute regime is given by[4,70]

$$R_g = R_{\text{end-to-end}}/\sqrt{6} \tag{4}$$

where

$$R_{\text{end-to-end}} \approx bN^{3/5}(cb^3)^{-1/5}K^{-2/5}(1 + 2Jc_s/c)^{-1/5} \tag{5}$$

The salt concentration c_s in a salt-free solution is $c_s = 4 \times 10^{-6}$. Debye lengths λ_D were taken from the calculations in section 3.2. In order to compare the experimental interchain distance to the theoretically predicted one, the CP-AFM d *vs* the calculated $2R_g$ and $2(R_g + \lambda_D)$ values for N = 20, 32, 64, and 155 are presented in Figures 7a and 7b, respectively. As expected, twice the sum of R_g predicts significantly smaller interchain distances. In case of $2(R_g + \lambda_D)$, the good agreement between the experimental and theoretical values is obvious. However, first of all this agreement depends highly on the choice of theoretical parameters J and K. Second, this relation does not lead to a scaling law with an exponent of −1/3 since λ_D scales with the concentration as $c^{-1/2}$. That means the deviation between the theoretical and the experimental values would increase by increasing or decreasing the studied concentration range. Third, there is no physical meaning behind this equation since the Debye length λ_D is just a mathematical description of the potential decay which depends on the ionic strength. In contrast to that, no effect of salt concentration could be detected for the center-to-center distance in the case of particles[8] or polymers.[29]

Another way to theoretically predict the interchain distance in the dilute regime is to simply calculate it through the particle number density *PND*, which would be $(c \times V/N)$, where V is the unit volume. The intercoil distance then would be $(c \times V/N)^{-1/3}$. The assumption here is that the coils never overlap with each other and that they have a symmetrical spherical volume. Figure 7c shows the experimental d from CP-AFM and the calculated intercoil distances from *PND*, for the NaPSS samples which were suggested to be in the dilute regime (N = 20−155). $2\pi/q_{max}$ from SAXS is not shown in the plot for the sake of clarity. A very good agreement between the calculated intercoil distances and experimental ones can be seen, explaining the dependence of the interchain distance on the chain length in the dilute regime. Unlike the calculations using the scaling theory, *PND* calculations do not depend on the microscopic parameters; they always give a scaling of $d \sim c^{-1/3}$, agreeing with the experimental results, and therefore they are a better tool to predict the intercoil distance in the dilute regime.

3.5. Viscosity Measurements. The rheological properties of polyelectrolyte solutions are determined by their configuration

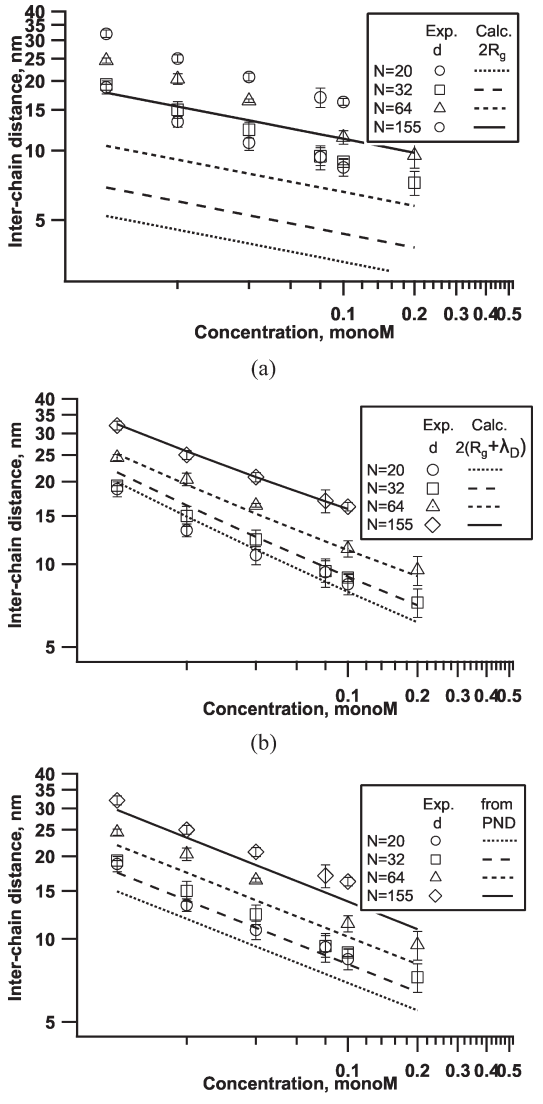

Figure 7. Experimental interchain distances as measured by CP-AFM (symbols) and the theoretical ones (lines) calculated by (a) $2R_g$ and (b) $2(R_g + \lambda_D)$ with the parameters $J = 5$ and $K = 2.8$ in eq 4 and (c) the particle number density (*PND*).

relative to each other[21] and highly depend on the type of structuring. The concentration dependence of the specific viscosity ($(\eta - \eta_s)/\eta_s$ where η is the measured viscosity and η_s is the solvent viscosity) is shown in Figure 8 for NaPSS with different chain lengths N and at various concentrations. For a fixed N, the specific viscosity increases with increasing monomer concentration, and at a fixed monomer concentration, it increases with increasing N.[4,21,22] In order to learn more about the structuring, scaling of the viscosity with monomer concentration was determined. As proposed by theory[4,22] and experiments,[21,71] the dependence of specific viscosity on c is given as

$$(\eta - \eta_s)/\eta_s \sim \begin{cases} c^{2/5} & \text{dilute—interacting} \\ c^{1/2} & \text{semidilute—unentangled} \\ c^{3/2} & \text{semidilute—entangled} \end{cases} \quad (6)$$

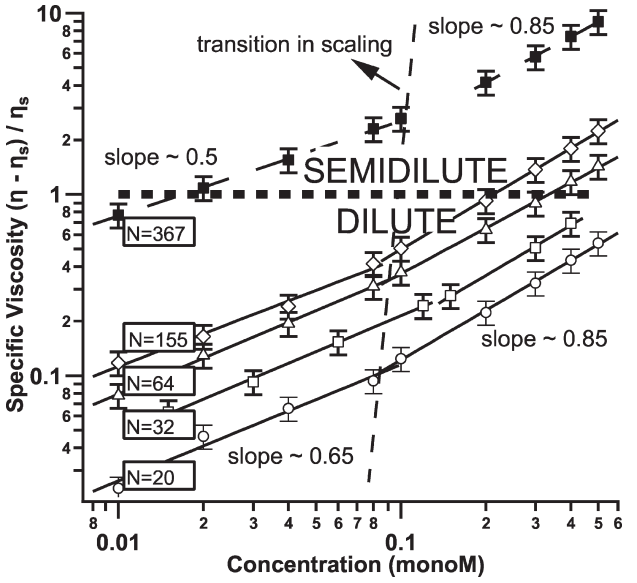

Figure 8. Measured viscosities of the NaPSS solutions with various chain lengths (symbols) and the linear fits in the log scale (lines). The thick dashed line shows the expected dilute—semidilute transition viscosity.

Generally, the change of the specific viscosity—monomer concentration dependence is reported to occur from $c^{1/2}$ to $c^{3/2}$, which was attributed to the semidilute—unentangled to —entangled transition.[4,6,21] This transition is expected to occur at the entanglement concentration c^{**} where[22] $\eta \approx 10$ to $100 \times \eta_s$, corresponding to[4] 10^3—$10^4 \times c^*$ (see Table 2). Interestingly, in the literature this transition always occurs at around a monomer concentration of 0.1 M independent of the NaPSS chain length.[21,71,72] Reviewing a wide set of literature work on rheology and dynamics of polymers, Colby[22] extracted a dependence of $c^{**} \sim N^{0.44}$. Unexpectedly, our results suggest a change in the $(\eta - \eta_s)/\eta_s$ vs c dependence at a concentration of around 0.1 M even for the dilute systems, which are far away from reaching c^{**}. The viscosity—concentration scaling ~0.65 (see Figure 8) for $c <$ 0.1 M in the dilute regime ($N = 20$—155) does not agree with the theoretical value of 2/5. The reason for this deviance is not clear but can be attributed to a stronger interaction between the NaPSS coils than predicted by the theory or unexpected charge distribution around the chains. The concentration dependence of the correlation lengths obtained from CP-AFM and SAXS on the monomer concentration should be noted at this point (section 3.2). For $c >$ 0.1 M, the scaling for N = 20 to 155 changes to 0.85, which could not be explained by the theory. For the semidilute regime sample $N = 367$, $\eta \sim c^{1/2}$ when $c <$ 0.1 M, agreeing with the theory. For $c >$ 0.1 M, however, this dependence becomes $\eta \sim c^{0.85}$, suggesting neither an unentangled nor an entangled structuring. A scaling between 1/2 and 3/2 in this regime was observed previously as was summarized elsewhere[21,22] but not yet explained by the theory. A reasonable explanation can be that the transition in the scaling between the unentangled— and entangled—semidilute regimes is not sharp, and around the transition concentration, it starts to increase starting from 1/2 and reaches to 3/2 at a higher concentration.

It was also suggested that the overlap concentration, c^*, is reached when $\eta \approx 2 \times \eta_s$, i.e., $(\eta - \eta_s)/\eta_s = 1$.[4,21,22] The thick dashed line in Figure 8 shows the specific viscosity = 1, the

theoretical dilute−semidilute transition viscosity. Figure 8 suggests that no such transition for samples with $N = 20$, 32, and 64 should occurs in the studied concentration regime. For $N = 155$, a transition should occur at a monomer concentration around 0.2 M, nearly at the same overlap concentration of 0.1 M calculated by the theory in section 3.4 (see Table 2). However, neither CP-AFM nor SAXS results indicated such a transition.

4. CONCLUSION

The ordering of monodisperse NaPSS samples in a wide range of chain lengths (N = 20−10 690) was studied in confined geometry with CP-AFM and in bulk with SAXS and viscosity measurements. Three different ordering parameters could be identified: (a) The interchain distance corresponds to the force period (confinement) and the inverse position of the scattering maximum (bulk). (b) The correlation length of the ordering corresponds to the force decay length and the inverse width of the structure peak. (c) The strength of the ordering is indicated by the amplitude of the force oscillation and the amplitude of the structure peak. While in case of the former two parameters the values obtained in confinement can be directly compared to the bulk values, the force and the scattering amplitude can be only compared in a qualitative way. The following conclusions are made:

(1) The confinement does not trigger a general change in the structural behavior for nonadsorbing NaPSS chains regardless of the concentration regime. In addition, the ordering on a mesoscopic length scale studied by CP-AFM and SAXS is directly correlated to the macroscopic properties reflected by the viscosity. All three methods, CP-AFM, SAXS, and viscosity measurements as well as theoretical calculations showed that in the studied concentration regime (0.01−0.5 M) the shorter chains up to 155 monomers are in the dilute regime (interchain distance $\sim c^{-1/3}$) while the longer chains overlap and form meshlike networks as expected for a semidilute system (interchain distance $\sim c^{-1/2}$).

(2) The confinement effect is detectable by an occurrence of force oscillations below a certain distance between the outer solid surfaces. In addition to that, a slight compression of the chains by a maximum 20% and an increase of counterion condensation at the PSS chains could be detected due to confinement.

(3) The assignment of the studied NaPSS concentrations to the *dilute* regime with a coil-like ordering and the *semidilute* regime with a network-like structuring are supported by the obtained result, that the interchain distance d depends on the degree of polymerization N in case of the dilute regime but not in the semidilute regime.

(4) The interchain distance, i.e., the center-to-center distance between the coils in the dilute regime, can be estimated by the coil number density. It is larger than twice the radius of gyration R_g, which would be expected for the dilute system. R_g is calculated based on model assumptions. The difference between $2 \times R_g$ and the intercoil distance is about twice the Debye length λ_D. Since there is no physical reason that the distance between two coil "surfaces" should be $2\times \lambda_D$ and the center-to-center distance should be $2(R_g + \lambda_D)$, it is assumed that this finding is specific for the studied concentration regime and cannot be generalized to a broader concentration regime. Another argument against the description of d by $d = 2(R_g + \lambda_D)$ is that the calculation is based on many assumptions with respect to the values of R_g and λ_D. In addition, in many former publications no effect of salt on the interchain distance in polyelectrolyte solutions[29] or on the particle distance in silica suspensions[8] could be detected.

(5) An increase in molecular weight leads to an increase in counterion condensation, which is detected as an increase in correlation length. The correlation length is longer than the Debye length, calculated under the assumption of counterion condensation. In contrast to Si suspensions where the particle radius and the Debye length are well-defined, a clear statement about the interchain distance and the Debye length cannot be made in case of polyelectrolytes. This is due to the fact that a polymer coil has quite an open structure.

(6) The strength of ordering increases with the degree of polymerization due to entropic reasons.

AUTHOR INFORMATION

Corresponding Author

*E-mail: klitzing@mailbox.tu-berlin.de. Phone: +49-30-314-23476. Fax: +49-30-314-26602.

ACKNOWLEDGMENT

We thank our colleague Yan Zeng for valuable discussions. DFG (IGRTG 1524) and Technical University of Berlin are acknowledged for the financing.

REFERENCES

(1) Degennes, P.; Pincus, P.; Velasco, R.; Brochard, F. *J. Phys. (Paris)* **1976**, *37*, 1461–1473.
(2) Odijk, T. *Macromolecules* **1979**, *12*, 688–693.
(3) Barrat, J.; Joanny, J. *Europhys. Lett.* **1993**, *24*, 333–338.
(4) Dobrynin, A.; Colby, R.; Rubinstein, M. *Macromolecules* **1995**, *28*, 1859–1871.
(5) Liao, Q.; Dobrynin, A. V.; Rubinstein, M. *Macromolecules* **2003**, *36*, 3386–3398.
(6) Dobrynin, A.; Rubinstein, M. *Prog. Polym. Sci.* **2005**, *30*, 1049–1118.
(7) Klapp, S. H. L.; Zeng, Y.; Qu, D.; von Klitzing, R. *Phys. Rev. Lett.* **2008**, *100*, 118303.
(8) Klapp, S. H. L.; Grandner, S.; Zeng, Y.; von Klitzing, R. *J. Phys.: Condens. Matter* **2008**, *20*, 494232.
(9) Grandner, S.; Zeng, Y.; von Klitzing, R.; Klapp, S. H. L. *J. Chem. Phys.* **2009**, *131*, 154702.
(10) Klapp, S. H. L.; Grandner, S.; Zeng, Y.; von Klitzing, R. *Soft Matter* **2010**, *6*, 2330–2336.
(11) Zeng, Y.; von Klitzing, R. *Soft Matter* **2011**, *7*, 5329–5338.
(12) Degennes, P. *Macromolecules* **1981**, *14*, 1637–1644.
(13) Khokhlov, A.; Khachaturian, K. *Polymer* **1982**, *23*, 1742–1750.
(14) Yethiraj, A.; Shew, C. *Phys. Rev. Lett.* **1996**, *77*, 3937–3940.
(15) Yethiraj, A. *J. Chem. Phys.* **1999**, *111*, 1797–1800.
(16) Netz, R.; Andelman, D. *Phys. Rep.* **2003**, *380*, 1–95.
(17) Milling, A.; Kendall, K. *Langmuir* **2000**, *16*, 5106–5115.
(18) Theodoly, O.; Tan, J.; Ober, R.; Williams, C.; Bergeron, V. *Langmuir* **2001**, *17*, 4910–4918.
(19) Jonsson, B.; Broukhno, A.; Forsman, J.; Akesson, T. *Langmuir* **2003**, *19*, 9914–9922.
(20) Rapoport, D. H.; Anghel, D. F.; Hedicke, G.; Moehwald, H.; von Klitzing, R. *J. Phys. Chem. C* **2007**, *111*, 5726–5734.
(21) Boris, D.; Colby, R. *Macromolecules* **1998**, *31*, 5746–5755.
(22) Colby, R. H. *Rheol. Acta* **2010**, *49*, 425–442.

(23) Nierlich, M.; Williams, C.; Boue, F.; Cotton, J.; Daoud, M.; Farnoux, B.; Jannink, G.; Picot, C.; Moan, M.; Wolff, C.; Rinaudo, M.; Gennes, P. *J. Phys. (Paris)* **1979**, *40*, 701–704.
(24) Nierlich, M.; Boue, F.; Lapp, A.; Oberthur, R. *J. Phys. (Paris)* **1985**, *46*, 649–655.
(25) Kaji, K.; Urakawa, H.; Kanaya, T.; Kitamiru, R. *J. Phys. (Paris)* **1988**, *49*, 993–1000.
(26) Baigl, D.; Ober, R.; Qu, D.; Fery, A.; Williams, C. *Europhys. Lett.* **2003**, *62*, 588–594.
(27) Nishida, K.; Kaji, K.; Kanaya, T. *Macromolecules* **1995**, *28*, 2472–2475.
(28) Nishida, K.; Kaji, K.; Kanaya, T. *J. Chem. Phys.* **2001**, *115*, 8217–8220.
(29) von Klitzing, R.; Kolaric, B.; Jaeger, W.; Brandt, A. *Phys. Chem. Chem. Phys.* **2002**, *4*, 1907–1914.
(30) Qu, D.; Baigl, D.; Williams, C.; Mohwald, H.; Fery, A. *Macromolecules* **2003**, *36*, 6878–6883.
(31) Qu, D.; Pedersen, J. S.; Garnier, S.; Laschewsky, A.; Moehwald, H.; von Klitzing, R. *Macromolecules* **2006**, *39*, 7364–7371.
(32) Koene, R.; Mandel, M. *Macromolecules* **1983**, *16*, 220–227.
(33) Drifford, M.; Dalbiez, J. *J. Phys. Chem.* **1984**, *88*, 5368–5375.
(34) Sedlak, M.; Amis, E. *J. Chem. Phys.* **1992**, *96*, 826–834.
(35) Sedlak, M.; Amis, E. *J. Chem. Phys.* **1992**, *96*, 817–825.
(36) Kleshchanok, D.; Tuinier, R.; Lang, P. R. *J. Phys.: Condens. Matter* **2008**, *20*, 073101.
(37) Biggs, S.; Prieve, D.; Dagastine, R. *Langmuir* **2005**, *21*, 5421–5428.
(38) Asnacios, A.; Espert, A.; Colin, A.; Langevin, D. *Phys. Rev. Lett.* **1997**, *78*, 4974–4977.
(39) Kolaric, B.; Jaeger, W.; von Klitzing, R. *J. Phys. Chem. B* **2000**, *104*, 5096–5101.
(40) von Klitzing, R.; Espert, A.; Asnacios, A.; Hellweg, T.; Colin, A.; Langevin, D. *Colloids Surf., A* **1999**, *149*, 131–140.
(41) von Klitzing, R.; Espert, A.; Colin, A.; Langevin, D. *Colloids Surf., A* **2001**, *176*, 109–116.
(42) Langevin, D. *Eur. Phys. J. E* **2001**, *5*, 81–85.
(43) Kleinschmidt, F.; Stutbenrauch, C.; Delacotte, J.; von Klitzing, R.; Langevin, D. *J. Phys. Chem. B* **2009**, *113*, 3972–3980.
(44) Milling, A. *J. Phys. Chem.* **1996**, *100*, 8986–8993.
(45) Biggs, S.; Dagastine, R.; Prieve, D. *J. Phys. Chem. B* **2002**, *106*, 11557–11564.
(46) Qu, D.; Brotons, G.; Bosio, V.; Fery, A.; Salditt, T.; Langevin, D.; von Klitzing, R. *Colloids Surf., A* **2007**, *303*, 97–109.
(47) Knoben, W.; Besseling, N. A. M.; Stuart, M. A. C. *Phys. Rev. Lett.* **2006**, *97*, 068301.
(48) Knoben, W.; Besseling, N. A. M.; Stuart, M. A. C. *Langmuir* **2007**, *23*, 6095–6105.
(49) Ribeiro, W.; Orfao, M.; Mata, J. L.; Saramago, B. *J. Colloid Interface Sci.* **2008**, *317*, 536–543.
(50) Stubenrauch, C.; von Klitzing, R. *J. Phys.: Condens. Matter* **2003**, *15*, R1197–R1232.
(51) Bonaccurso, E.; Kappl, M.; Butt, H.-J. *Curr. Opin. Colloid Interface Sci.* **2008**, *13*, 107–119.
(52) Üzüm, C.; Kristen, N.; von Klitzing, R. *Curr. Opin. Colloid Interface Sci.* **2010**, *15*, 303–314.
(53) von Klitzing, R.; Thormann, E.; Nylander, T.; Langevin, D.; Stubenrauch, C. *Adv. Colloid Interface Sci.* **2010**, *155*, 19–31.
(54) Delacotte, J.; Rio, E.; Restagno, F.; Uzum, C.; von Klitzing, R.; Langevin, D. *Langmuir* **2010**, *26*, 7819–7823.
(55) Kim, S.-C.; Suh, S.-H.; Seong, B.-S. *J. Chem. Phys.* **2007**, *127*, 114903.
(56) Yang, S.; Tan, H.; Yan, D.; Nies, E.; Shi, A.-C. *Phys. Rev. E* **2007**, *75*, 061803.
(57) Burns, J.; Yan, Y.; Jameson, G.; Biggs, S. *J. Colloid Interface Sci.* **2002**, *247*, 24–32.
(58) Biggs, S.; Burns, J.; Yan, Y.; Jameson, G.; Jenkins, P. *Langmuir* **2000**, *16*, 9242–9248.
(59) Biggs, S. *Phys. Chem. Chem. Phys.* **2010**, *12*, 4172–4177.
(60) Ducker, W.; Senden, T.; Pashley, R. *Nature* **1991**, *353*, 239–241.
(61) Riegler, H.; Engel, M. *Ber. Bunsen. Phys. Chem.* **1991**, *95*, 1424–1430.
(62) Helm, C. A.; Möhwald, H.; Kjaer, K.; Als-Nielsen, J. *Biophys. J.* **1987**, *52*, 381–390.
(63) Evans, R.; Henderson, J.; Hoyle, D.; Parry, A.; Sabeur, Z. *Mol. Phys.* **1993**, *80*, 755–775.
(64) Piech, M.; Walz, J. *J. Phys. Chem. B* **2004**, *108*, 9177–9188.
(65) Limbach, H.; Holm, C.; Kremer, K. *Europhys. Lett.* **2002**, *60*, 566–572.
(66) Manning, G. *J. Chem. Phys.* **1969**, *51*, 924–933.
(67) Milling, A.; Vincent, B. *J. Chem. Soc., Faraday Trans.* **1997**, *93*, 3179–3183.
(68) Nikolov, A.; Wasan, D. *J. Colloid Interface Sci.* **1989**, *133*, 1–12.
(69) Nikolov, A.; Wasan, D. *Langmuir* **1992**, *8*, 2985–2994.
(70) Rubinstein, M.; Colby, R. *Polymer Physics*; Oxford University Press: Oxford, 2003.
(71) Prini, R.; Lagos, A. *J. Polym. Sci., Part A* **1964**, *2*, 2917–&.
(72) Chen, S.; Archer, L. *J. Polym. Sci., Polym. Phys.* **1999**, *37*, 825–835.